Journal of Applied Geophysics 80 (2012) 101–109

Contents lists available at SciVerse ScienceDirect

Journal of Applied Geophysics

journal homepage: www.elsevier.com/locate/jappgeo

Measuring the dielectric properties of soil–organic mixtures using coaxial impedance dielectric reflectometry

Franco M. Francisca *, Marcos A. Montoro

Consejo Nacional de Investigaciones Científicas y Técnicas (CONICET), and Universidad Nacional de Córdoba (UNC), Vélez Sarsfield 1611, 5016, Córdoba, Argentina

ARTICLE INFO

Article history:
Received 26 May 2011
Accepted 30 January 2012
Available online 10 February 2012

Keywords:
NAPL
Soil pollution
Detection
Dielectric permittivity
Effective mixture model
Soil heterogeneity

ABSTRACT

Contamination of soils with non-aqueous phase liquids (NAPLs) is frequently produced by accidental spills and storage tanks or pipes leakage. The main goals dealing with soil and groundwater contamination include determining the extension of the affected zone, monitoring the contaminant plume and quantifying the pollution degree. The objective of this work is to evaluate the potential of dielectric permittivity measurements to detect the presence of NAPLs in sands. Tested samples were fine, medium, coarse and silty sand with different volumetric contents of water and paraffin oil. The dielectric permittivity was measured by means of a Coaxial Impedance Dielectric Reflectometry method in specimens with either known fluid content or at different stages during immiscible displacement tests. A simplified method was developed to quantify the amount of oil from dielectric permittivity measurements and effective mixture media models. Obtained results showed that groundwater contamination with NAPL and the monitoring of immiscible fluid displacement in saturated porous media can be clearly identified from dielectric measurements. Finally, very accurate results can be obtained when computing the contamination degree with the proposed method in comparison with the real volumetric content of NAPL ($r^2 > 90\%$).

1. Introduction

Soils are porous media composed by multiple phases including mineral particles, water and air. Organic contaminants in contact with soils divide between the water, air and mineral phases and sometimes form a separate phase which is recognized as non-aqueous phase liquid (NAPL). Detection of NAPL and the monitoring of contaminated plumes are of fundamental importance in geoenvironmental studies.

The effort to detect organic contaminants in soils is increasing since the last ten years. The monitoring and mapping of contaminated soil frequently involve geophysical prospecting methods as complement of conventional geological, chemical and hydrological studies (Garcia–Gonzalez et al., 2008; Knight, 2001). Non-destructive geophysical techniques help to rapidly detect contaminants in soils and to monitor the extension of polluted areas (Carcione et al., 2003). Electric methods based on the propagation/reflection of electromagnetic waves have been successfully used in the past to detect organic contaminants in soils (Ajo-Franklin et al., 2006; Shinn et al., 1998). However, detection is restricted to sites with spatial and temporal variations of the complex dielectric permittivity of soils and high contamination levels (Brewster et al., 1995; Hwang et al., 2008; Kaya and Fang, 1997; Wilson et al., 2009).

Dielectric measurements are useful to estimate water and oil content within porous media (Liu and Mitchell, 2009; Persson and Haridi, 2003; Topp et al., 1980). The presence of liquid organic contaminants in soils can be identified due to their different dielectric, physical and chemical properties with respect to pore water (Ajo-Franklin et al., 2006; Moroizumi and Sasaki, 2008; Son et al., 2009). Although previous studies showed that NAPL affects the complex permittivity of soils, little concern has been given to the effect of medium heterogeneities and the spatial variability of NAPL saturation on computed concentrations of contaminants.

The purpose of this study is to investigate the correlation between the volumetric content of NAPL and the dielectric permittivity of sandy soils. The objectives include the analysis of the dielectric behavior of saturated sands contaminated with NAPL, the monitoring and detection of anomalies and trapped oil by measuring the dielectric permittivity with a Coaxial Impedance Dielectric Reflectometry sensor, and the development of a simplified procedure to determine the volumetric content of NAPL by means of dielectric permittivity measurements. These will provide new results useful to interpret geophysical field data and to quantify the presence of organic contaminants by means of non-destructive dielectric measurements.

2. Complex permittivity of soils

The relative permittivity (κ^*) of heterogeneous porous media is a complex parameter defined as:

$$\kappa^* = \frac{\varepsilon^*}{\varepsilon_0} = \kappa' - j\ \kappa'' \tag{1}$$

* Corresponding author. Tel.: +54 351 4334404 (199).
E-mail address: ffrancis@efn.uncor.edu (F.M. Francisca).

0926-9851/$ – see front matter © 2012 Elsevier B.V. All rights reserved.
doi:10.1016/j.jappgeo.2012.01.011

where the real and imaginary components are:

$$\kappa' = \frac{\varepsilon'}{\varepsilon_0} \tag{2}$$

$$\kappa'' = \frac{\varepsilon''}{\varepsilon_0} + \frac{\sigma_0}{\omega\ \varepsilon_0} \tag{3}$$

and $j=\sqrt{-1}$, ε' and ε'' are real and imaginary permittivity, respectively, ε_0 is the free space permittivity (8.85×10^{-12} F/m), ω is the angular frequency and σ_o is the conductivity at zero frequency (DC).

The permittivity of soils depends on the volumetric content and permittivity of each phase, particle shape and orientation, phase distribution, interaction between phases and the frequency of measurements (Endres and Knight, 1991; Robinson and Friedman, 2002; Wobschall, 1977). In the megahertz frequency range a relaxation of soil permittivity arises when electrical charges accumulate at interfaces and borders (Arulanandan and Smith, 1973). This mechanism can be very important in fine soils (silts and clays) but has irrelevant significance in water-wet sands (Rinaldi and Francisca, 1999; Saarenketo, 1998), dry soils (Ulaby et al., 1990), and soils saturated with NAPL (Francisca and Rinaldi, 2003).

Effective medium models consider that the effective complex permittivity (κ^*_{eff}) of phase mixtures depends on the permittivity and volumetric content of each of phase (Kärkkäinen et al., 2000; Van Beek, 1967). Different mixing models predict different effective permittivity for the same soil. The simplest mixture formulae consider that:

$$\kappa^{*\,c}_{eff} = \sum_i \frac{V_i}{V}\ \kappa^{*c}_i \tag{4}$$

where κ^*_i and V_i are the permittivity and volume of the '*i*' phase respectively, V is the total volume, and c is a constant that varies from −1 to 1 depending on the geometrical arrangement of the components (Lichtenecker and Rother, 1931). The fitting parameter c usually ranges from 0.4 to 0.8 for soil mixtures (Jacobsen and Schjønning, 1995), when $c=0.5$ the model is known as Complex Refractive Index Mixture (CRIM) and applies for isotropic mediums, and if $c=1/3$ the Eq. (4) becomes equal to the Looyenga's model (Van Beek, 1967). Francisca and Rinaldi (2003) compiled effective medium models frequently used for analyzing the dielectric permittivity of soils. These models can be used to predict the dielectric properties of contaminated soils by extending them to four-phase mixtures (particles, water, contaminant and air). Recently, Seyfried et al. (2005) presented a simplified equation to determine the water volumetric content of soils from the measured dielectric permittivity as follows:

$$\theta_w = A\sqrt{\kappa^*_{eff}} + B \tag{5}$$

where A and B are fitting parameters. These authors successfully fitted the model to 19 different soil samples capturing the influence of saturation and soil texture on dielectric permittivity.

The displacement of immiscible liquids inside the pores modifies the complex permittivity of soils. The dielectric properties of NAPL are characterized by $\kappa'\approx2$ and $\kappa''\approx0$ due to the low polarizability and conductivity of these liquids, which results in a low capacity to dissolve in water and associate with other elements. The NAPL displaces either air ($\kappa'=1$; $\kappa''=0$) or water ($\kappa'\approx78.5$ and $\kappa''>0$) when penetrating in the soil pores and consequently modifies κ^*_{eff} (Darayan et al., 1998; Kaya and Fang, 1997; Son et al., 2009). When NAPL ($\kappa'\approx2$) displaces water ($\kappa'\approx78.5$) in saturated soils, the change in dielectric permittivity is easily detected (Rinaldi and Francisca, 2006). However, detection of immiscible displacement becomes difficult in the case of unsaturated soil when a liquid with $\kappa'\approx2$ replaces the air ($\kappa'=1$) in the soil pores. In this case, the initial dielectric properties of the soil and a complimentary measurement of contamination are required. The phase distribution and wetting conditions can also affect the permittivity of soil–water–organic mixtures (Santamarina and Fam, 1997). This phenomenon is significant when testing clay–water–oil mixtures given that the presence of oil and the mixing order can affect the development of the diffuse double layer around clay particles.

Commonly employed techniques to measure soil's dielectric permittivity in the megahertz frequency range include time domain reflectometry (TDR), ground penetrating radar (GPR), resonant frequency modulation devices, coaxial transmission lines, and impedance-network analyzers. The three first techniques can be applied both, at field or laboratory scale, while the last ones provide very accurate laboratory data (Benson and Bosscher, 1999; Cassidy, 2007; Francisca and Rinaldi, 2003; Knight, 2001). There were many efforts to correlate and upscale dielectric permittivity measurements from the field to the laboratory with limited success (Brewster et al., 1995; Carcione et al., 2003). The main identified problems are related to the spatial variability of soil properties and biodegradation effects (Johnston et al., 2007; Kao and Prosser, 2001,).

Geoenvironmental applications of geophysical techniques based on electromagnetic wave propagation frequently include detection of contaminant in soils and monitoring of contaminant plumes. The spatial variability of soil dielectric impedance, which is mainly controlled by the spatial variability of soil type, porosity and moisture content, is the main limiting factor for the identification of dielectric features that could be associated with contaminants in soil pores. However, if the dielectric permittivity of an aquifer at a given place is known before the infiltration of organic contaminants, any change in dielectric properties can be associated with the contaminant migration.

3. Laboratory methods

3.1. Dielectric permittivity measurements

The complex dielectric permittivity was measured with the Hydra Probe Coaxial Impedance Dielectric Reflectometry probe manufactured by Stevens Water Monitoring Systems Inc. This sensor has four metal rods or tines; three of them define a cylindrical measurement volume of 2.5 cm in diameter and 6 cm in length, and the fourth rod is in the center of this sensing volume [Fig. 1(a)]. The tines are used to measure the complex dielectric permittivity and a temperature sensor is placed in the probe head. The probe can be placed under the water table and in contact with contaminant substances for very long times without suffering damage.

The equipment generates a 50 MHz electromagnetic wave that propagates as a planar waveguide to the tines and reflects from the sensing volume creating a standing wave as in a coaxial transmission line. The reflected signal depends on the probe impedance which in turn depends on the dielectric properties of the material in the sensing volume (Campbell, 1990).

The sensor accuracy to measure the real and imaginary component of the dielectric permittivity of the material in the measurement region is ±1% (or ±0.5). The dielectric permittivity response of the sensor is linear with the contact length of the rods with the tested material (Seyfried et al., 2005), which allows identifying anomalies when the measurement are conducted by gradually inserting the probe in the soil.

The dielectric permittivity is determined from three measured voltages, but unfortunately, the equation that relates the voltages to the dielectric permittivity is not provided by the manufacturer (Blonquist et al., 2005). The volumetric water content, soil salinity, soil conductivity and pore water conductivity are computed from the real and imaginary dielectric permittivities (Stevens Vitel, 1994). The soil type under test should be selected given that the equipment has three specific calibration curves, for sand silt and clay, to compute moisture content.

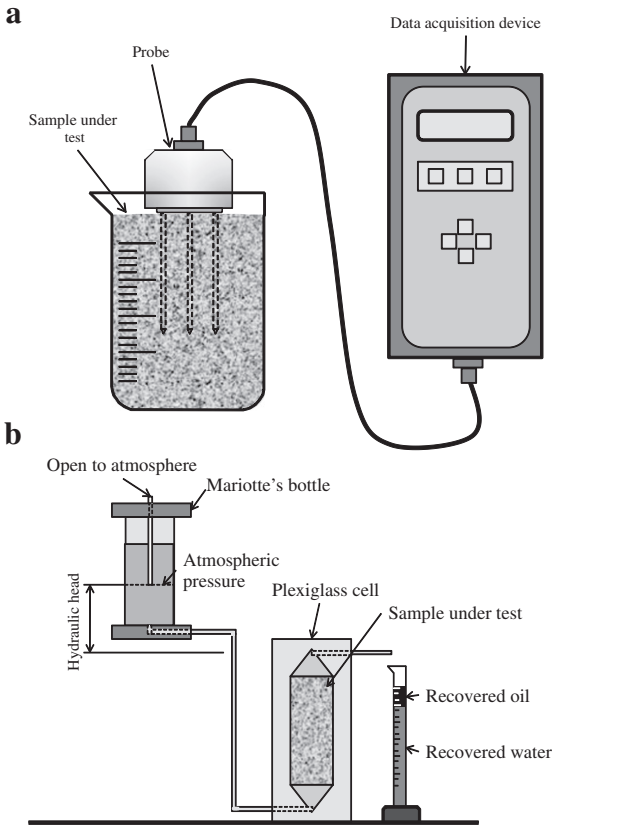

Fig. 1. a) Schematic representation of the Coaxial Impedance Dielectric Reflectometry sensor and measurement procedure; b) experimental setup used in the immiscible displacement tests.

Seyfried and Murdock (2004) determined that the dielectric permittivity of fluids can be accurately measured with the Hydra Probe sensor and reported coefficient of variations for their results lower than 1%. In addition, dielectric permittivities measured with the Hydra Probe sensor compare very well with that measured with other commercial electromagnetic probes (Blonquist et al., 2005).

3.2. Tested materials

The tested soils are coarse, medium, fine and silty sands. Table 1 presents their relevant properties determined by following the American Society for Testing and Materials (ASTM) standards for soils (ASTM, 2007). The coarse, medium and fine sand are poorly graded and classify as SP while the silty sand is also poorly graded and corresponds to SP-SM in the unified soil classification system. Silty sand was prepared by mixing 75% of coarse sand and 25% of loessical silt from Cordoba (Argentina). Most common exchangeable cations found in silt samples are Ca^{2+} (3–12 me/100 g), Mg^{2+} (2–6 me/100 g), Na^{+} (1–15 me/100 g) and K^{+} (1–3 me/100 g) (Rinaldi and Cuestas, 2002).

Table 1
Physical properties of the soils.

Property	Sand			
	Fine	Medium	Coarse	Silty
Mean particle size (μm)	410	425	1000	750
Particle size<0.6 mm (%)	64	59	24	43
Particle size<0.2 mm (%)	15	26	3.50	27
Particle size<0.074 mm (%)	2.07	1	1.28	23.32
Clay content (<0,002 mm) (%)	0	0	0	2.32
Specific gravity	2.68	2.68	2.68	2.66
Specific surface [m^2/g]	0.001–0.04	0.001–0.04	0.001–0.04	0.15

The fluids selected to prepare the mixtures were deionized water and paraffin oil. The paraffin oil has a relative density of 0.84 and a real dielectric permittivity of 2.1.

3.3. Experimental procedure

Two different experiments were performed to characterize the dielectric properties of soil–fluid mixtures and to verify the displacement of organic liquids inside soil pores. The first group of experiments refers to dielectric permittivity measurements conducted in mixtures with known volumetric content of either water or paraffin oil. The second group of experiments refers to dielectric permittivity measurements conducted in samples initially saturated with paraffin oil and then flushed with colored water.

Soil mixtures were prepared with the soils oven dried at 105 °C and mixed with different gravimetric content of the liquid (w). Three different groups of mixtures were prepared: a) soil–water, b) soil–paraffin oil and c) soil–water–paraffin oil. The specimens were placed in a cylindrical glass cup 50 mm in diameter and 100 mm in height, and weighted to obtain their total unit weight (γ) which was carefully controlled. The size of the beaker used to hold the specimen was higher than the measurement volume of the probe to avoid boundary effects.

The presence of each fluid phase was characterized by means of the volumetric content (θ) which is a dimensionless ratio between the volume of the fluid phase respect to the total volume. The volumetric fluid content can be obtained from the unit weight of the soil (γ, the unit weight of water (γ_w) and the gravimetric fluid content (w):

$$\theta = \frac{V_i}{V} = \frac{w}{\gamma_w}\frac{\gamma}{(1+w)} = nS \tag{6}$$

where V_i is the volume of any liquid phase, V is the total volume of the sample, n is the porosity and S is the degree of saturation. Subscript "w" or "o" can be used to identify the fluid type inside the pores (e.g. water or oil). It is important to note that when the soil is fully saturated with either water or oil ($S=1$), the fluid volumetric content is equal to porosity ($\theta=n$).

The dielectric properties of the mixture were obtained by carefully introducing the probe tines in the soil sample placed in the graduated cylindrical cup [Fig. 1(a)]. Negligible changes in the total volume of the soil were detected when introducing the tines in the sample and no volume changes were observed during the dielectric permittivity measurements.

The second group of experiments was designed to monitor the removal of organic contaminants from the oil saturated soil [Fig. 1(b)]. The test procedure included the following stages. A testing cell of 7 cm in width, 7 cm in height and 14 cm in length was filled with sand contaminated with paraffin oil. Then the specimen was permeated with the same organic fluid to obtain a saturation degree close to one. An auxiliary cell (Mariotte's bottle) contains the water colored with fluorescein which was used to displace the paraffin oil from the soil. A constant hydraulic gradient equal to one was used to force the penetration of water inside the sample from bottom to top. Because the cell wall is transparent the displacing of paraffin oil by colored water was directly visualized. Water and paraffin oil permeated through the sample were collected in the outlet port. The volume of fluids permeated trough the sample was taken as a reference parameter to monitor oil displacement and water and paraffin oil saturations.

The volumes of the displacing fluid permeated through the sample were varied in order to evaluate the dielectric properties of specimens with different residual saturation of paraffin oil. The dimensionless number known as pore volume of flow (N_{pv}) was used to allow for

the ratio between the volumes of displacing fluid (V_d) and resident fluid (V_v) during the immiscible displacement test:

$$N_{PV} = \frac{V_d}{V_v} \tag{7}$$

At the end of each removal test, the cell was placed in horizontal position, the top cap was removed and the permittivity was measured by carefully introducing the dielectric probe in the specimen in 21 different places. The measurement locations were selected such as the 21 sensing volumes have small overlap with each other, and two additional determinations were placed in coincidence with the inlet and outlet areas (see online supplementary material). This procedure provides average dielectric properties for the material within the sensing volume. The measured dielectric permittivity was attributed to the central point of the sensing volume in order to create the dielectric permittivity maps. This procedure allowed capturing the spatial variability of dielectric permittivity in the horizontal direction in the specimen.

There is a very small overlap between the sensing volume and the cell wall for some of the measurements positions (online supplementary material). The boundary effect on the dielectric measurements and maps was verified by testing medium sand saturated with water. The mean and standard deviation of κ' were 21.5 and 1.1, respectively. The obtained standard deviation could be responsible for scatters lower than 2% on the computed water content which is lower than the number of significant digits for this soil properties according to the ASTM D6026 (ASTM, 2007), In addition, the obtained dielectric map shown in the online supplementary material, reveals an uniform pattern of dielectric permittivities and negligible boundary effects.

Digital pictures were acquired at different stages during the immiscible displacement tests. These pictures were processed in order to enhance the contrast between areas saturated with water and areas saturated with paraffin oil. The image analysis was used as a complementary technique to detect the presence of oil. Image analysis provides local information about the fluid distribution at the specimen surface while dielectric measurements provide average volumetric properties for the sensing volume. Qualitative image analysis allowed justifying observed changes in dielectric permittivity measurements.

Immiscible displacement tests were also performed in three heterogeneous specimens that were: a) medium sand with a cylindrical inclusion of silty sand perpendicular to the flow direction, b) medium sand with a cylindrical inclusion of hydrophobic medium sand perpendicular to the flow direction, and c) a layer of hydrophobic sand in between of two layers of hydrophilic sand, oriented parallel to the flow direction.

The hydrophilicity of the sand was modified to favor the affinity between soil particles and paraffin oil. Hydrophobic sand was prepared by coating sand particles with a thin film of silicone and then drying the particles at 105 °C during 24 h. The hydrophobicity was checked by pouring the sand in water and verifying that the particles remained dry due to water repellency after 24 h of immersion.

For the special case of the layered sample, the dielectric permittivity measurements were conducted by gradually introducing the sensor tines in order to detect changes in the dielectric properties at different depths. The distribution of the measuring sites is the same shown in the Online Supplementary Material. In these measurements, the probe is gradually introduced in the sample and therefore the tines are in part in contact with air and in part in contact with the specimen under test. The measured dielectric permittivity is expected to be linear with the penetration length as stated by Seyfried et al. (2005). Changes in the dielectric properties of the material produce deviations respect to the linear response of the probe.

Forces involved during immiscible displacement are capillary, gravity and viscous forces. The relative contribution of these forces during immiscible flow is measured by means of three dimensionless numbers: the capillary number N_c which relates capillary to viscous forces, the bond number N_B which relates capillary to gravity forces and the trapping number N_T which relates capillary to the bond number (Pennell et al., 1996). The lowest computed values for these dimensionless numbers at the end of the immiscible displacement tests were $N_c = 1.3\times10^{-7}$, $N_B = 4\times10^{-6}$ and $N_T = 4\times10^{-6}$ (coarse sand). According to Gioia and Urciolo (2006) there are no ganglia movement in the porous media for $N_B < 1.2\times10^{-3}$ and $N_c < 2\times10^{-4}$. Therefore, no redistribution of fluids is expected during the dielectric permittivity measurements.

4. Results and analysis

4.1. Heterogeneous-phase mixtures

Fig. 2 shows the variation of κ' and κ'' of the coarse, medium and fine sands and the silt with the volumetric content of water or paraffin oil. The volumetric contents were computed by measuring the unit weight of the sample (γ), moisture content, (w) and using Eq. (6). The real and imaginary permittivity increases with the volumetric content of fluid phase since used liquids have higher real permittivity than air ($\kappa_a' = 1$). This increase is higher in the case of water ($\kappa' \approx 78.5$) in comparison with the paraffin oils ($\kappa' = 2.10$), as expected according to Eq. (4). The imaginary component increases with the volumetric content only in the case of water but displays near to zero values in all the sand–paraffin oil mixtures.

Fig. 2 also shows a comparison between the measured data and Topp et al. (1980) and Seyfried et al. (2005) models (Eqs. (8) and (5), respectively) for the soil–water mixtures. The models proposed by Francisca and Rinaldi (2003) (Eq. (9)) and Seyfried et al. (2005) (Eq. (5)) for soil–paraffin oil mixtures are also included as reference.

$$\kappa_{sw}' = 3.03 + 9.3\theta_w + 146\theta_w^{\,2} - 76.7\theta_w^{\,3} \tag{5}$$

$$\kappa_{so}' = 2.232 + 2.188\ \theta_{po} \tag{6}$$

The measured dielectric permittivity in sand–water mixtures are adequately predicted by Topp et al. (1980) model. Seyfried et al. (2005) model was successfully fitted to the experimental data and allowed distinguishing soil textures. The fitting parameters obtained for the sand–water mixtures were $A = 0.115$ and $B = -0.184$, while for silt–water mixtures were $A = 0.0931$ and $B = -0.1896$. These values are in good agreement with those reported by Seyfried et al. (2005) for similar soils. In the case of soil–paraffin oil mixtures, Francisca and Rinaldi (2003) and Seyfried et al. (2005) models accurately predicted to the measured data and the fitting parameters of Seyfried et al. (2005) model resulted $A = 0.6708$ and $B = -0.989$.

Some of the scatter in the data can be in part attributed to the effect of sample porosity as predicted by Eq. (4) and most of effective media models (Zakri et al., 1998), and in part to the accuracy of the sensor. Very similar κ' and κ'' values were measured for the fine, medium and coarse sands regardless the volumetric content of either water or paraffin oil. The observed differences were lower than the accuracy of the probe. The effect of phase distribution or mixing order on dielectric permittivity is considered negligible given that tested soils have low specific surface and the amount of water in the diffuse double layer can be neglected.

Both real and imaginary permittivities of silt–water mixtures were higher than for the fine, medium and coarse sands given that at 50 MHz the measurement captured the last part of an interfacial polarization mechanism and due to the higher conductivity of the silt fraction controlled by the presence and mobility of ions (Rinaldi and Francisca, 1999).

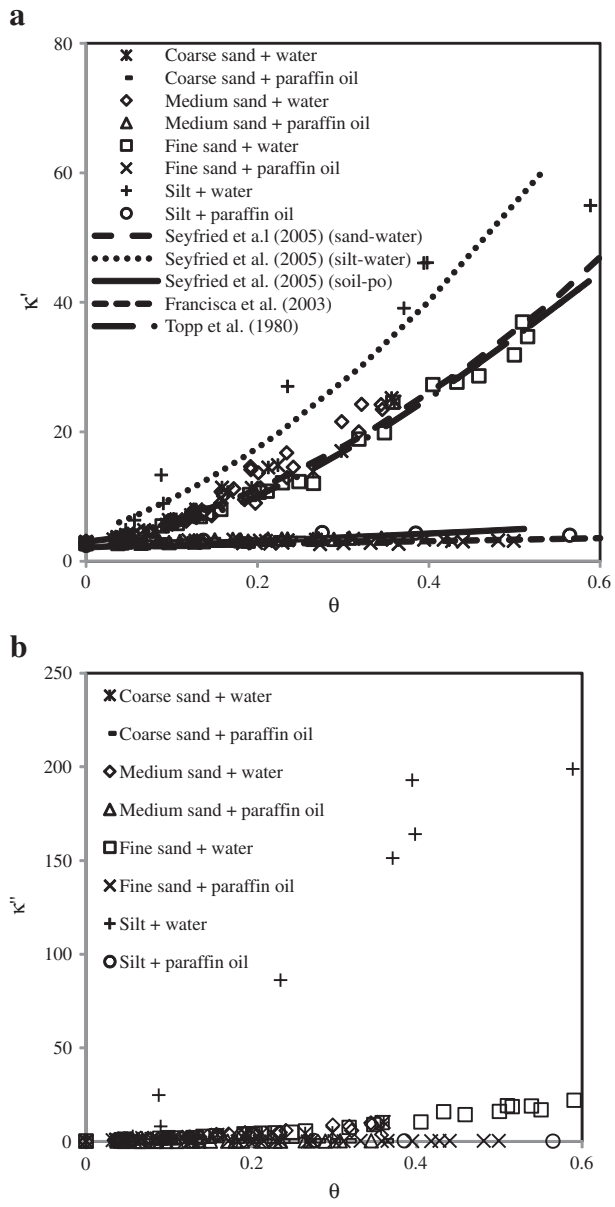

Fig. 2. Influence of the volumetric content of fluids on soil dielectric properties. a) Real dielectric permittivity, b) Imaginary dielectric permittivity.

4.2. Anomaly detection in macroscopic homogeneous samples

Fig. 3 shows the results obtained in immiscible displacement tests performed in medium sand. The specimen was initially saturated with paraffin oil and then permeated with colored water. Figs. 3(a) and (b) present contrast enhanced pictures of the visible face [Fig. 1(b)] after flushing when the $N_{pv}=1$ and $N_{pv}=20$, respectively, and Figs. 3(c) and (d) show the corresponding real dielectric permittivity maps.

The measured real permittivities after $N_{pv}=1$ range from 3.08 to 9.92 while after 20 pore volumes of flow were between 17.42 and 21.07. The higher values of κ' are attributed to the replacement of the organic liquid ($\kappa'=2.1$) by the displacing fluid ($\kappa'=78.65$) and the volumetric content of water (θ_w) and oil (θ_o). After the oil displacement the samples still remain completely saturated. Then, the processed digital pictures shown in Fig. 3 indicate that more paraffin oil was displaced by water when κ' has higher values. In addition, the observed difference between the maximum and minimum values of κ' at each state corresponds to regions with different volume of oil (lower κ' is expected in areas with paraffin oil ganglia which are trapped blobs of the NAPL). Similar trends were obtained for the imaginary component of the dielectric permittivity.

25 tests were performed in macroscopic homogeneous specimens of fine, medium, coarse and silty sand, with varying volume of displacing fluid (V_d) used to displace the paraffin oil. In general, all specimens showed similar characteristics after finishing the displacement test and the obtained κ' and κ'' maps had similar features to the one shown in Fig. 3. The displacement of paraffin oil by colored water and the presence of trapped oil were confirmed by visual observations through the transparent cell wall.

Fig. 4 shows the variation of the mean κ' and κ'' values between the 21 measurement positions with the pore volume of flow. The displacement of paraffin oil by water visually observed was also detected by the dielectric measurements. Both components of permittivity increase with the amount of fluid used to displace the contaminants approaching the values measured in clean saturated sand. The difference between the κ' measured after flushing and the κ' measured in clean sand indicates that some oil still remains inside the pores.

4.3. Anomaly detection in macroscopic heterogeneous samples

Fig. 5 shows a contrast enhanced picture of the visible face and the κ' and κ'' maps after 20 pore volumes of flow obtained for the mean sand with a cylindrical inclusion of silty sand, while Fig. 6 presents similar data for the same sand with a cylindrical inclusion of hydrophobic sand. Visual observations confirmed that in both cases there were clear accumulations of water at the interface between materials with different capillarity (Das et al., 2004; Van Duijn et al., 2007). In

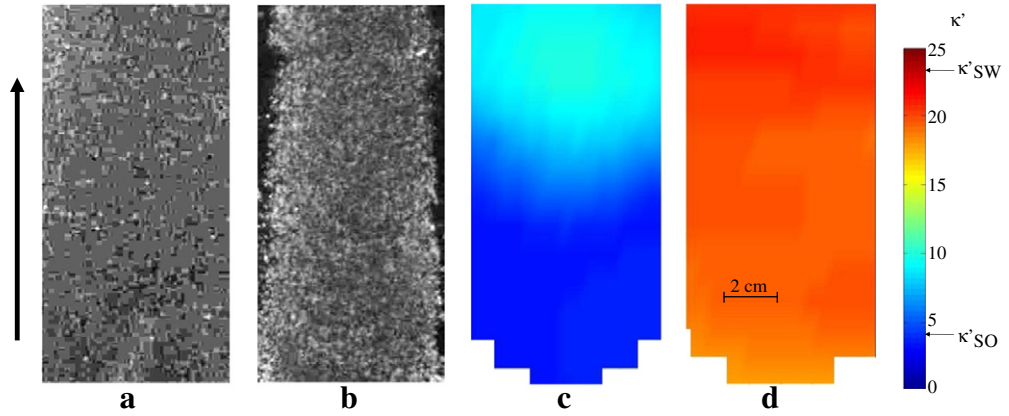

Fig. 3. Displacement test performed in the medium sand initially contaminated with paraffin oil. a) Contrast enhanced picture of the visible face at $N_{pv}=1$; b) Contrast enhanced picture of the visible face at $N_{pv}=20$, black = paraffin oil invaded pixel and white = colored water invaded pixel; c) Real dielectric permittivity map, $N_{pv}=1$; d) Real dielectric permittivity map, $N_{pv}=20$. The arrow indicates flow direction.

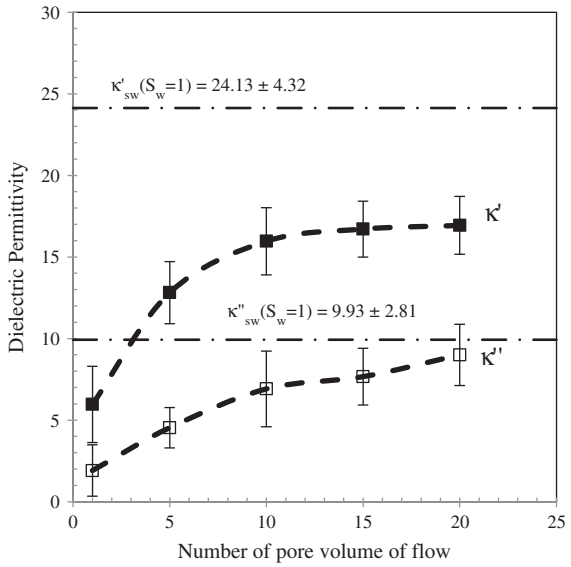

Fig. 4. Influence of the immiscible displacement of paraffin oil by water on the dielectric permittivity of medium sand. Error bars represent the standard deviation between the 21 measurement positions.

addition, higher amount of paraffin oil trapped in the cylindrical inclusion was qualitatively confirmed by means of visual observations and image analysis.

The real permittivity measured in the silty sand inclusion reaches values slightly lower than that observed in the sample body [Fig. 5(b)]. This result indicates that a higher amount of paraffin oil is being trapped in the silty sand pores. Similar trends are observed in the dielectric permittivity map of the hydrophilic sand with the hydrophobic sand inclusion where the local occlusion of NAPL is promoted by the affinity between the hydrophobic sand grains and the organic fluid [Fig. 6(b)]. These trends are in good agreement with visual observations and image analysis of the exposed face of the specimen under test. Note that changes in dielectric permittivity could be attributed to soil texture, bulk density, saturation degree and dielectric permittivity of the pore fluid. In order to distinguish the effect of texture from contamination, the initial dielectric permittivity should be known in advance, or soil layers with homogeneous soil textures should be identified by means of any complimentary technique. When all soil properties remain constant, any change in dielectric permittivity can be attributed to changes in the type and volumetric content of pore fluid.

The higher saturations of oil in the silty sand and hydrophobic sand inclusions are also inferred from the imaginary dielectric permittivity maps [Figs. 5(c) and 6(c)]. Very clear higher κ'' values are observed in coincidence with the anomaly given that the imaginary permittivity of the sand saturated with water is $\kappa''\approx 10$ while in the case of silty sand saturated with this liquid is $\kappa''\sim 150$. The κ'' in the silty sand lens was close to 35 after the displacement process which confirmed that water invaded the pores of this material given that the κ'' of paraffin oil saturated silt resulted close to zero [Fig. 2(c)]. The κ'' measurements also capture the presence of the hydrophobic sand inclusion even that hydrophilic and hydrophobic sands have practically the same permittivity. Hence, the pattern observed in the permittivity map shown in Fig. 6(c) confirms the presence of trapped oil in the cylindrical inclusion of hydrophobic sand.

The dielectric permittivity of the medium sand surrounding the cylindrical inclusions resulted slightly different in Figs. 5b and 6b; even the samples were prepared by following the same experimental procedure. The average increase in κ' of the sand surrounding the silty sand and the hydrophobic sand was from 3.1 to 18.6 and from 3.1 to 14.2 respectively, and was attributed to the replacement of paraffin oil by water. This result confirms that the specimens considered macroscopically homogeneous are heterogeneous porous media at micro scale (Lenormand et al., 1988; Sahimi, 1993). The residual paraffin oil saturation after immiscible displacement resulted 0.11 and 0.19 for the samples with the silty sand and hydrophobic sand inclusions, respectively. These residual oil contents, computed from the volume of oil collected in the outlet port, are in good agreement with the observed increases of κ'.

Fig. 7a shows an upper view and two cross sections of the tested specimen. Typical distributions of paraffin oil in the direction perpendicular to the flow path can be observed in the cross sections A-A and B-B. The hydrophobic sand layer in the middle of the specimen has a darker color which is produced by the higher content of paraffin oil. Fig. 7b displays the influence of the probe penetration on κ' and κ'' in this layered specimen. The intervals represent two standard deviations of the experimental κ' and κ''. The real and imaginary permittivities increased with the depth of penetration and displayed a change in the rate of increase as expected in materials with different dielectric permittivities. The lower increase rate of κ' and κ'' determined in the middle of the specimen is produced by the higher volume of paraffin oil entrapped due to the hydrophobicity of this layer. In addition, the

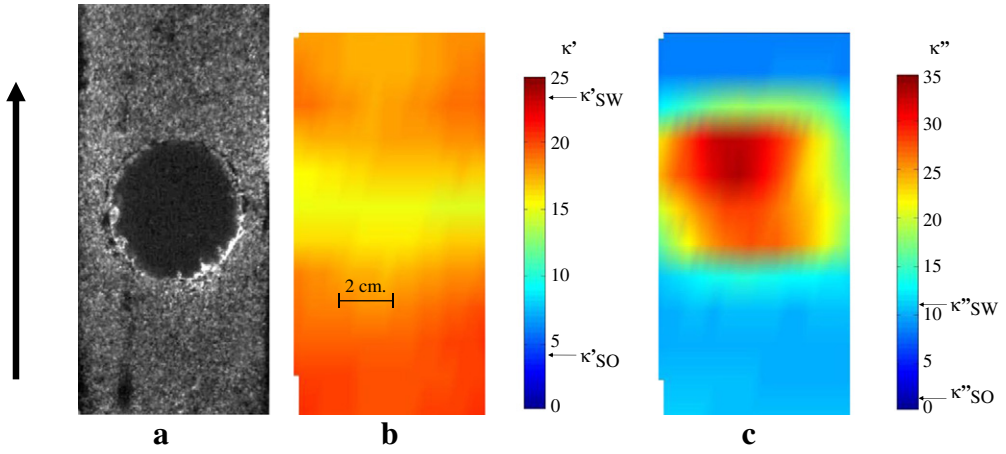

Fig. 5. Displacement test performed in the medium sand initially contaminated with paraffin oil with a cylindrical inclusion of silty sand. a) Contrast enhanced picture of the visible face at $N_{pv}=20$, black = paraffin oil invaded pixel and white = colored water invaded pixel; b) Real dielectric permittivity map; c) Imaginary permittivity map. The arrow indicates flow direction.

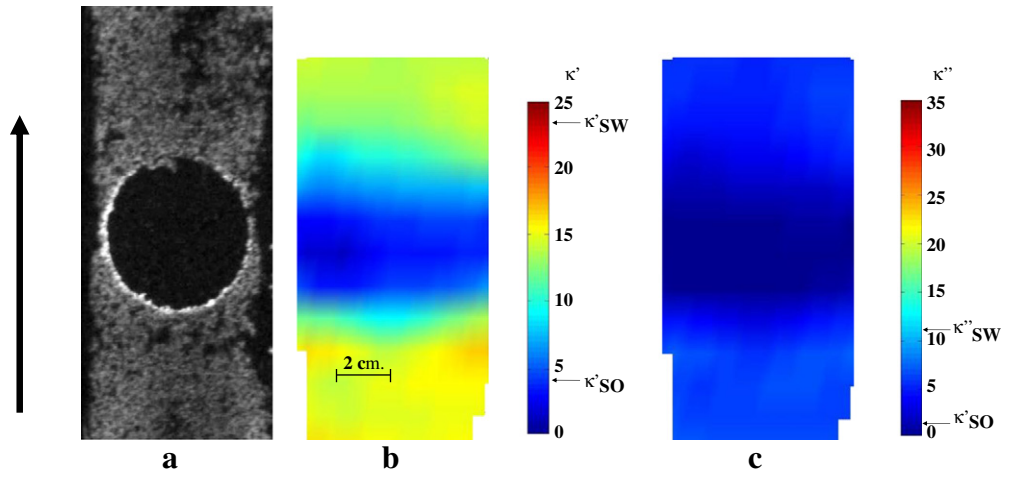

Fig. 6. Displacement test performed in the medium sand initially contaminated with paraffin oil with a cylindrical inclusion of hydrophobic sand. a) Contrast enhanced picture of the visible face at $N_{pv}=20$, black = paraffin oil invaded pixel and white = colored water invaded pixel; b) Real dielectric permittivity map; c) Imaginary permittivity map. The arrow indicates flow direction.

scatter of data increases significantly with the penetration, as a result of the presence of ganglia in the three soil layers. The random distribution of trapped oil ganglia in the two hydrophilic sand layers and the absence of a perfectly abrupt interface between the hydrophilic–hydrophobic and the hydrophobic–hydrophilic strata are responsible of the observed deviations with respect to the expected linear behavior of the probe (Seyfried et al., 2005).

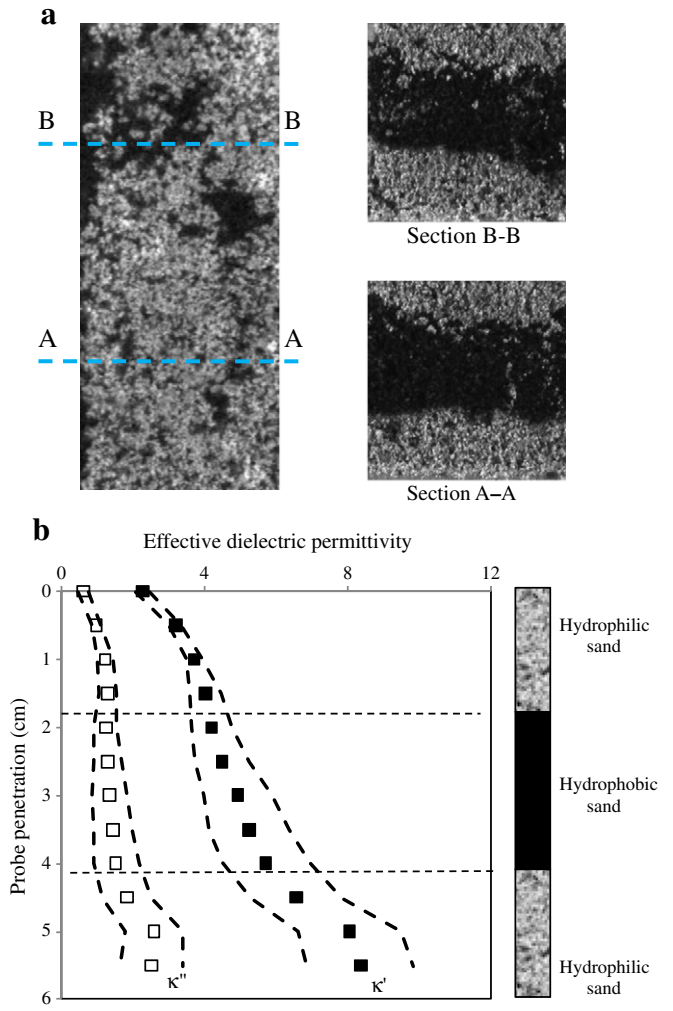

Fig. 7. Displacement test performed in a layered system. a) Contrast enhanced picture of the sample surface (upper view) and two cross sections (A-A and B-B) after $N_{pv}=20$; black = paraffin oil invaded pixel and white = colored water invaded pixel; b) Dielectric permittivity profile determined after $N_{pv}=20$.

5. Discussion

5.1. Indirect estimation of paraffin oil volumetric content

The effect of paraffin oil content on the real dielectric permittivity of saturated sands was evaluated by testing specimens where the volumetric content of oil (θ_o) added to the volumetric content of water (θ_w) is equal to the sample porosity ($n=\theta_w+\theta_o$). Fig. 8 shows the real permittivity and volumetric content measured in saturated specimens prepared with known volumetric content but different θ_w and θ_o. Measurements performed in the specimens tested in the multiphase flow experiments are also included in Fig. 8. The upper and lower limits of dielectric permittivity which corresponds to sand–water and sand–paraffin oil mixtures, respectively, are the best fit curves from the calibration presented in Fig. 2. Since the specimens are saturated ($S=1$) the volumetric content of fluids equals porosity (Eq. (6)). The real permittivity falls in between the two boundaries which means that real permittivities lower than that measured in the sand–water mixtures indicate the presence of paraffin oil.

The simultaneous effect of soil porosity and volumetric content on κ' and κ'' can be obtained from any effective media model. According to Eq. (4) and adopting $c=0.5$ changes in porosity can produce changes in κ' as high as 140%; while for saturated soils, a change in the fluid dielectric permittivity from 78.5 (e.g. water) to 2.1 (e.g. paraffin oil) reduces the expected κ'_{eff} by 920%.

Effective media models need to be extended from two to three phase mixtures in order to model the dielectric response of contaminated soils. Alternatively, if the dielectric response of soil–water (κ_{sw}') and soil–organic mixtures (κ_{so}') is known the dielectric permittivity at a given volumetric content can be determined as:

$$\kappa'^{\,c}_{m} = \alpha\ \kappa'^{\,c}_{so} + (1-\alpha)\kappa'^{\,c}_{sw} \tag{10}$$

where κ'_{sw} and κ'_{so} are real permittivities of sand–water and sand–paraffin oil mixtures, measured at the same liquid volumetric content for the specimen under test, α is the relative amount of organic contaminated sand mixed with clean water saturated sand, and c is a fitting parameter included to maintain similarity with Eq. (4). Note that: a) κ'_{sw} and κ'_{so} are obtained from previous measurements or calibration curves as the ones shown in Fig. 2(a), b) the soil porosity (n) of saturated soils

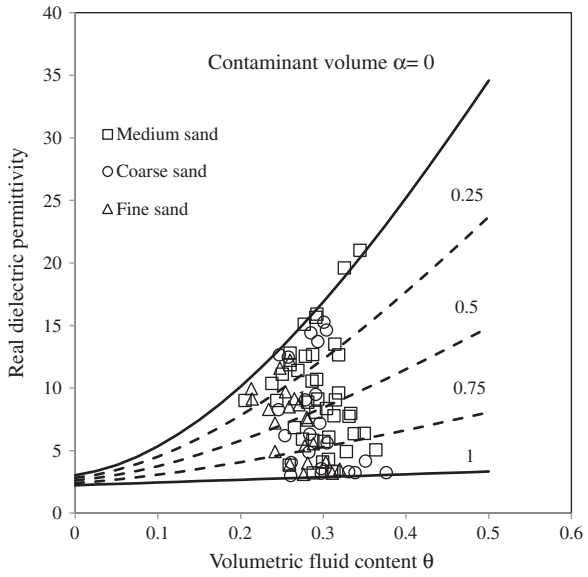

Fig. 8. Real dielectric permittivity of water–paraffin oil–sand mixtures with known volumetric composition.

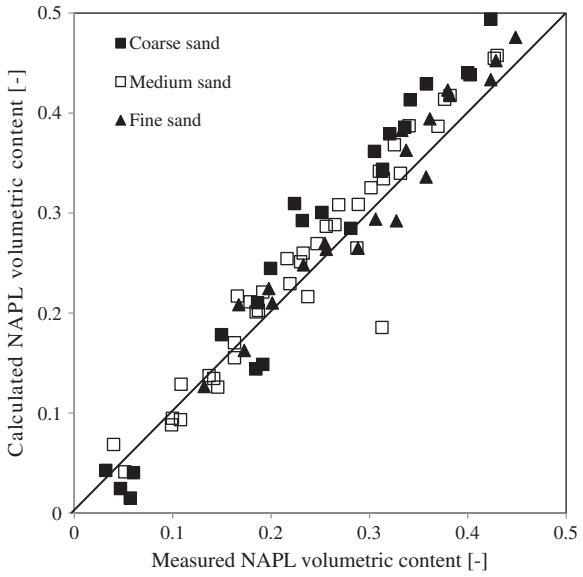

Fig. 9. Calculated and measured volumetric content of paraffin oil in sand–water–paraffin oil mixtures.

can be obtained from the grains specific gravity (G_s) and dry unit weight (γ_d) as follows:.

$$n = 1 - \frac{\gamma_d}{G_s \gamma_w} \tag{11}$$

Then, α varies from 0 to 1 and becomes equal to the relative volume of paraffin oil in the liquid phase:

$$\alpha = \frac{\theta_o}{\theta_w + \theta_o} \tag{12}$$

Eq. (10) with $c = 0.5$ was used to predict the dielectric response of soil samples contaminated with different relative volumes of paraffin oil ($\alpha = 0$, 0.25, 0.5, 0.75 and 1). These theoretical results are presented in the same Fig. 8. Lower dielectric permittivities are predicted when the relative volume of paraffin oil increases due to the lower real permittivity of paraffin oil ($\kappa' = 2.10$) with respect to that of water ($\kappa' = 78.65$). Predicted permittivities when the extreme values $\alpha = 0$ and $\alpha = 1$ are adopted became equal to the experimental permittivity of sand–water and sand–paraffin oil mixtures, respectively. The effect of κ'' was ignored because sand–water and sand–NAPL mixtures are low loss materials.

The volumetric content of paraffin oil was computed from Eqs. (10) and (12) with κ'_{sw} and κ'_{so} from Fig. 2(a), the dielectric permittivity measured in the contaminated sample (κ'_m) and assuming $c = 0.5$ (alike in CRIM formula). Then, this provides a simplified way to predict θ_o from the κ'_m and the permittivities κ'_{sw} and κ'_{so} measured at the same θ. Instead, real oil contents were known from the initial volume of paraffin oil added to the specimens, sample porosity ($n = \theta_o$) and the volume of oil recovered after soil washing. Fig. 9 compares the volumetric content of paraffin oil computed from Eqs. (10) and (12) with the known volumetric content. These results include the saturated specimens prepared with different amount of oil and water and those obtained from the immiscible displacement tests. The trend line has an $r^2 = 0.91$ meaning that the methodology proposed in this study has a very high precision (or accuracy in predicting α).

This result confirms the potential of the dielectric permittivity measurements to detect NAPL in soils and the possibility of estimating the volumetric content of NAPL by knowing the dielectric behavior of soil–water mixtures and soil–NAPL mixtures. Identified limitations of the proposed method to compute the amount of organic fluids inside soil are: a) soil porosity and the frequency of measurements must be constants; b) Eq. (10) is valid only for low loss materials, otherwise the imaginary permittivity must be considered in the analysis; and c) soil samples should be saturated. Hence, detection is restricted only to the volumetric content of NAPL since the organic fraction dissolved in water, adsorbed to the solid phase or in the air inside the pores cannot be detected with this technique.

Obtained results confirmed that the proposed measurements and analysis can be used for the development of early spill monitoring system for buried oil pipes and tanks. Detection of leakage and soil contamination could be performed by placing the coaxial dielectric reflectometry probe below the pipes and tanks, and monitoring changes in the dielectric permittivity of the soil. In addition, the volumetric content of organic contaminants could be determined from calibration curves similar to those shown in Fig. 2, soil porosity, the initial dielectric permittivity and the change in dielectric permittivity associated to the saturation of pores with oil.

6. Conclusions

This investigation presents experimental results of dielectric permittivity measurements to detect the contamination of soils with NAPL. Dielectric permittivity measurements allow determining the presence of liquids with different κ' and κ'' inside soil pores. Given that soils are multiphase mixtures, the effective dielectric permittivity depends on the volumetric content of the pore fluid. For the tested sands, the effective dielectric permittivity increases with the volumetric content of water or paraffin oil for clean and contaminated sand, respectively. Obtained results are in good agreement with expected values according to the models developed by Topp et al. (1980) for water–sand mixtures, and Francisca and Rinaldi (2003) for oil–sand mixtures. In addition, the model proposed by Seyfried et al. (2005) fitted well the experimental results and allowed capturing the influence of soil texture on the dielectric properties of soil–water and soil–paraffin oil mixtures.

The dielectric permittivity of soils contaminated with NAPL depends on soil porosity, volumetric content of water and NAPL, and degree of saturation. The dielectric permittivity of phase mixture can be evaluated by effective media models. In order to compute the volume of NAPL, the permittivity of fully cleaned and fully contaminated saturated sand specimens and soil porosity must be previously known. The analysis proposed in this research allows estimating oil contents from dielectric

permittivity measurements that well correlate with the real volumetric content of the contaminant inside soil pores ($r^2 > 90\%$).

Dielectric measurements can be used for the monitoring of NAPL displacement in porous media. The immiscible displacement, directly observed and monitored with image processing, modifies the dielectric properties of soils. This allows evaluating the evolution of the NAPL saturation degree during remediation processes and computing the organic content at different stages during remediation.

In the case of heterogeneous materials, the presence of interfaces can be detected by analyzing the linear dependence between effective dielectric permittivity and penetration of the sensor tines. This is relevant for the detection of anomalies and for the identification of zones with higher amount of occluded contaminants. The proposed methodology gives the possibility of study soil contamination and monitoring decontamination processes with fairly similar accuracy in laboratory and in-situ measurements. Obtained results provide significant information about the dielectric properties of heterogeneous soils contaminated with NAPL that can be used to improve data analysis from geophysical methods based on electromagnetic wave propagation.

Supplementary materials related to this article can be found online at doi:10.1016/j.jappgeo.2012.01.011.

Acknowledgements

This study was supported by CONICET, FONCyT and SECyT-UNC. M.A.M. received support from CONICET as Ph.D. candidate during this project. The authors also thank the anonymous reviewers for their valuable comments.

References

Ajo-Franklin, J.B., Geller, J.T., Harris, J.M., 2006. A survey of the geophysical properties of chlorinated DNAPLs. Journal of Applied Geophysics 59 (3), 177–189.
Arulanandan, K., Smith, S.S., 1973. Electrical dispersion in relation to soil structure. Journal of the Soil Mechanics and Foundation Division 99 (SM12), 1113–1133.
ASTM, 2007. Annual Book of ASTM Standards, Section 4: Construction. Soil and Rocks, Vol. 04.08. American Society for Testing and Materials.
Benson, C.H., Bosscher, P.J., 1999. Time-Domain Reflectometry (TDR) in Geotechnics: A Review. In: Marr, W.A., Fairhust, C.E. (Eds.), Nondestructive and Automated Testing for Soil and Rock Properties, ASTM, STP1350. American Society for Testing and Materials, West Conshohoken.
Blonquist, J.M., Jones, S.B., Robinson, D.A., 2005. Standardizing characterization of electromagnetic water content sensors: part 2. Evaluation of seven sensing systems. Vadose Zone Journal 4, 1059–1069.
Brewster, M.L., Annan, A.P., Greenhouse, J.P., Kueper, B.H., Olhoef, G.R., Redman, J.D., Sander, K.A., 1995. Observed migration of controlled DNAPL release by geophysical methods. Ground Water 3 (6), 977–987.
Campbell, J.J., 1990. Dielectric properties and influence of conductivity of soils at one to fifty megahertz. American Journal of Soil Science 54 (2), 332–341.
Carcione, J.M., Seriani, G., Gei, D., 2003. Acoustic and electromagnetic properties of soils saturated with salt water and NAPL. Journal of Applied Geophysics 52 (4), 177–191.
Cassidy, N.J., 2007. Evaluating NPAL contamination using GPR signal attenuation analysis and dielectric properties measurements: practical implications for hydrological studies. Journal of Contaminant Hydrology 94 (1–2), 49–75.
Darayan, S., Liu, C., Shen, L.C., Shatthuck, D., 1998. Measurement of electrical properties of contaminated soil. Geophysical Prospecting 46 (5), 477–488.
Das, D.B., Hassanizadeh, S.M., Rotter, B.E., Ataie-Ashtiani, B., 2004. A numerical study of micro-heterogeneity effects on upscaled properties of two-phase flow in porous media. Transport in Porous Media 56 (3), 329–350.
Endres, A., Knight, R., 1991. The effects of pore-scale fluid distribution on the physical properties of partially saturated tight sandstones. Journal of Applied Physics 69 (2), 1091–1098.
Francisca, F.M., Rinaldi, V.A., 2003. Complex dielectric permittivity of soil-organic mixtures (20 MHz–1.3 GHz). Journal of Environmental Engineering 129 (4), 347–357.
Garcia–Gonzalez, J.E., Ortega, M.F., Chacon, E., Mazadiego, L.F., De Miguel, E., 2008. Field validation of radon monitoring as screening methodology for NAPL-contaminated sites. Journal of Applied Geochemistry 23 (9), 2753–2758.
Gioia, F., Urciolo, M., 2006. Combined effect of bond and capillary numbers on hydrocarbon mobility in water saturated porous media. Journal of Hazardous Materials B133, 218–225.
Hwang, Y.K., Endres, A.L., Pigott, S.D., Parker, B.L., 2008. Long term ground penetrating radar monitoring for a small volume DNAPL release in a natural groundwater flow field. Journal of Contaminant Hydrology 97 (1–2), 1–12.
Jacobsen, O.H., Schjønning, P., 1995. Comparison of TDR calibration functions for soil water determination. Time-Domain Reflectometry Applications in Soil Science. Danish Institute of Plant and Soil Science, Lyngby, Denmark, pp. 25–33.
Johnston, C.D., Bastow, T.P., Innes, N.L., 2007. The use of biodegradation signatures and biomarkers to differentiate spills of petroleum hydrocarbon liquids in the subsurface and estimate natural mass loss. European Journal of Soil Byology 43 (5–6), 328–334.
Kao, C.M., Prosser, J., 2001. Evaluation of natural attenuation rate at a gasoline spill site. Journal of Hazardous Materials 82 (3), 275–289.
Kärkkäinen, K.K., Sihvola, A.H., Nikoskinen, K.I., 2000. Effective permittivity of mixtures: numerical validation by the FDTD method. IEEE Transactions on Geoscience and Remote Sensing 38 (3), 1303–1308.
Kaya, A., Fang, H.Y., 1997. Identification of contaminated soils by dielectric constant and electrical conductivity. Journal of Environmental Engineering 123 (2), 169–177.
Knight, R., 2001. Ground penetrating radar for environmental applications. Annual Review of Earth and Planetary Sciences 29, 229–255.
Lenormand, R., Touboul, E., Zarcone, C., 1988. Numerical models and experiments on immiscible displacement in porous media. Journal of Fluid Mechanics 189, 165–187.
Lichtenecker, K., Rother, K., 1931. Die Herleitung des logarithmischen Mischungsgesetzes aus allgemeinen Prinzipien der startionären Strömung. Physik Zeitschr 32, 255–260.
Liu, N., Mitchell, J.K., 2009. Effects of structural and compositional factors on soil electromagnetic properties. Geomechanics and Geoengineering 4 (4), 271–285.
Moroizumi, T., Sasaki, Y., 2008. Estimating the nonaqueous-phase liquid content in saturated sandy soil using amplitude domain reflectometry. Soil Science Society of America Journal 72 (6), 1520–1526.
Pennell, K.D., Pope, G.A., Abriola, L.M., 1996. Influence of viscous and buoyancy forces on the mobilization of residual tetrachloroethylene during surfactant flushing. Environmental Science and Technology 30 (4), 1328–1335.
Persson, M., Haridi, S., 2003. Estimating water content from electrical conductivity measurements with short time-domain reflectometry probes. Soil Science Society of America Journal 67 (2), 478–482.
Rinaldi, V.A., Cuestas, G.A., 2002. Ohmic conductivity of a compacted silty clay. Journal of Geotechnical and Geoenvironmental Engineering 128 (10), 824–835.
Rinaldi, V.A., Francisca, F.M., 1999. Impedance analysis of soil dielectric dispersion (1 MHz to 1 GHz). Journal of Geotechnical Engineering 125 (2), 111–121.
Rinaldi, V.A., Francisca, F.M., 2006. Removal of immiscible contaminants from sandy soils monitored by means of dielectric measurement. Journal of Environmental Engineering 132 (8), 931–939.
Robinson, D.A., Friedman, S.P., 2002. The effective permittivity of dense packing of glass beads, quartz sand and their mixtures immersed in different dielectric backgrounds. Journal of Non-Crystalline Solids 305 (1–3), 261–267.
Saarenketo, T., 1998. Electrical properties of water in clay and silty soils. Journal of Applied Geophysics 40 (1–3), 73–88.
Sahimi, M., 1993. Flow phenomena in rocks: from continuum models to fractals, percolation, cellular automata, and simulated annealing. Review of Modern Physics 65 (4), 1393–1537.
Santamarina, J.C., Fam, M., 1997. Dielectric permittivity of soils mixed with organic and inorganic fluids (0.02 GHz to 1.30 GHz). Journal of Environmental and Engineering Geophysics 2 (1), 37–51.
Seyfried, M.S., Murdock, M.D., 2004. Measurement of soil water content with a 50 MHz soil dielectric sensor. Soil Science Society of America Journal 68, 394–403.
Seyfried, M.S., Grant, L.E., Du, E., Humes, K., 2005. Dielectric loss and calibration of the hydra probe soil water sensor. Vadose Zone Journal 4 (4), 1070–1079.
Shinn, J.D., Timian, D.A., Morey, R.M., Hull, R.L., 1998. Development of a CPT probe to determine volumetric soil moisture content. In: Robertson, Mayne (Eds.), Proceedings of the First International Conference on Site Characterization ISC'98. Balkema, pp. 595–599.
Son, Y., Oh, M., Lee, S., 2009. Influence of diesel fuel contamination on the electrical properties of unsaturated soil at a low frequency range of 100 Hz–10 MHz. Environmental Geology 58 (6), 1341–1348.
Stevens Vitel, 1994. Hydra Soil Moisture Probe User's Manual.
Topp, G.C., Davis, J.L., Annan, A.P., 1980. Electromagnetic determination of soil water content: measurements in coaxial transmission line. Water Resources Research 16 (3), 574–582.
Ulaby, F., Bengal, T., Dobson, M., East, J., Garvin, J., Evans, D., 1990. Microwave dielectric properties of dry rocks. IEEE Transactions on Geoscience and Remote Sensing 28 (3), 325–336.
Van Beek, L.K., 1967. Dielectric behavior of heterogeneous systems. Progress in Dielectrics 7. John Wiley and Sons, NY, pp. 67–114.
Van Duijn, C.J., Eichel, H., Helmig, R., Pop, I.S., 2007. Effective equations for two-phase flow in porous media: the effect of trapping on the microscale. Transport in Porous Media 69 (3), 411–428.
Wilson, V., Power, C., Giannopoulos, A., Gerhard, J., Grant, G., 2009. DNAPL mapping by ground penetrating radar examined via numerical simulation. Journal of Applied Geophysics 69 (3–4), 140–149.
Wobschall, D., 1977. A theory of the complex dielectric permittivity of soil containing water: the semidispersed model. IEEE, Transaction on Geoscience Electronics 15 (1), 49–58.
Zakri, T., Laurent, J.P., Vauclin, M., 1998. Theoretical evidence for 'Lichtenecker's mixture formulae' based on the effective medium theory. Journal of Physics D: Applied Physics 31, 1589–1594.